A Ca^{2+}-regulated deAMPylation switch in human and bacterial FIC proteins.

Simon Veyron[1], Giulia Oliva[2,3], Monica Rolando[2,3], Carmen Buchrieser[2,3], Gérald Peyroche[1], Jacqueline Cherfils[1]

[1]Laboratoire de Biologie et Pharmacologie Appliquée, CNRS and Ecole normale supérieure Paris-Saclay, Cachan, France

[2] Institut Pasteur, Biologie des Bactéries Intracellulaires, Paris, France

[3] CNRS, UMR 3525, Paris, France

Correspondence to :

Jacqueline Cherfils
Laboratoire de Biologie et Pharmacologie Appliquée,
CNRS and Ecole normale supérieure Paris-Saclay,
61 Avenue du Président Wilson
94235 Cachan CEDEX, France
jacqueline.cherfils@ens-paris-saclay.fr

Abstract

FIC proteins regulate molecular processes from bacteria to humans by catalyzing post-translational modifications (PTM), the most frequent being the addition of AMP using ATP as a cofactor, a reaction coined AMPylation. In a large group of AMPylating FIC proteins, which includes single-domain bacterial FIC proteins and animal FICD/HYPE, AMPylation is intrinsically repressed by a structurally conserved glutamate. Curiously, FICD departs from previously characterized bacterial FIC proteins in that it acts bifunctionally to AMPylate and deAMPylate its target, the endoplasmic reticulum BiP/GRP78 chaperone. BiP is a key component of the unfolded protein response (UPR), and is AMPylated under normal conditions where its activity is low, while its activation correlates with its deAMPylation. Currently, a direct signal regulating AMPylation efficiency in bacterial and animal FIC proteins has not been identified. Here, we addressed this question for a FIC protein from the bacterial pathogen *Enterococcus faecalis* (EfFIC) and for human FICD. We discover that EfFIC catalyzes both AMPylation and deAMPylation within the same active site, suggesting that the conserved glutamate is the signature of AMPylation/deAMPylation bifunctionality. Crystal structures and PTM assays identify a multi-position metal switch implemented by the glutamate, whereby EfFIC uses Mg^{2+} and Ca^{2+} to control AMPylation and deAMPylation differentially without conformational change. Remarkably, we find that variations in Ca^{2+} levels also tune deAMPylation of BiP by human FICD. Together, our results identify metals as diffusible signals that can regulate bifunctional FIC proteins directly, and they suggest that FICD has features of an enzymatic sensor of Ca^{2+} depletion, a hallmark of the UPR.

Introduction

In less than a decade, FIC proteins have emerged as a large family of enzymes controling the activity of target proteins by post-translationally modifying them with phosphate-containing compounds (reviewed in [1,2,3,4]). These proteins are characterized by the presence of a conserved FIC domain, which carries out the post-translational modification (PTM) of a Tyr, Ser or Thr residue in a target protein [5,6,7,8,9,10,11]. The most frequent PTM reaction catalyzed by FIC enzymes is the addition of AMP using ATP as a cofactor, coined AMPylation or adenylylation. This PTM activity was originally discovered in toxins from bacterial intracellular pathogens [12] and was later identified in the toxin component of bacterial toxin/antitoxins modules (e.g. Bartonella VbhT/VbhA, [7]) and in various other bacterial FIC proteins of unknown functions, including single-domain (e.g. Neisseria FIC [7]) and larger (e.g. Clostridium FIC [11]) FIC proteins. Metazoans possess a single FIC protein, FICD/HYPE (FICD hereafter), which controls the reversible AMPylation of BiP/GRP78, an Hsp70 chaperone localized in the endoplasmic reticulum (ER) [13,14,15]. BiP is a major component of the unfolded protein response (UPR), a major pathway whereby cells respond to ER stress (reviewed in [16]). AMPylation of BiP reduces its affinity for unfolded protein clients [17] and inversely correlates with the burden of unfolded proteins [15]. In a recent twist, FICD was shown to act bifunctionally in both AMPylation and deAMPylation of BiP and to carry out deAMPylation as its primary enzymatic activity in vitro [18].

All PTM reactions catalyzed by FIC proteins use a motif of conserved sequence for catalysis, the FIC motif, which carries an invariant histidine that is critical for nucleophilic attack of the cofactor by the target residue, and an acidic residue (aspartate or glutamate) that binds an Mg^{2+} ion to stabilize the negative charges of the cofactor phosphates at the transition state (reviewed in [1,2,3,4]). A large group of FIC proteins also features a structurally conserved glutamate that represses AMPylation by protruding into the catalytic site from either N-terminal elements, as in human FICD [10], *Clostridum difficile* FIC [11] or *Shewanella oneidensis* FIC [19], or from a C-terminal α-helix as in single-domain FIC proteins from *Neisseria meningitidis* [7] and *Helicobacter pylori* (PDB 2F6S). Crystal structures showed that this glutamate prevents ATP from binding in a catalytically-competent conformation [7,11], while its mutation into glycine creates space for the γ-phosphate of ATP [7] and has been consistently shown to increase AMPylation activities *in vitro* and in cells (reviewed in [20]). These observations led to propose that this conserved glutamate represses AMPylation by impairing

the utilization of ATP as a donor for AMP, hence that it must be displaced to allow productive binding of ATP [7]. In *N. meningitidis* FIC (NmFIC), upregulation of the AMPylation activity was proposed to occur upon changes in the toxin concentration [21]. In this scheme, NmFIC is in an inactive tetrameric state at high concentration, which is further stabilized by ATP, while its dilution promotes its conversion into a monomeric state, leading to activation by displacement of the inhibitory glutamate followed by autoAMPylations that reinforce AMPylation efficiency [21]. Whether a similar mechanism applies to other glutamate-bearing FIC proteins has not been investigated. Remarkably, in bifunctional human FICD, the autoinhibitory glutamate is critical for deAMPYlation of the BiP chaperone [18], a reaction whereby FICD contributes to the activation of BiP under ER stress conditions. Currently, a signal that represses the deAMPylation activity of FICD under normal ER conditions has not been identified. Together, these intriguing observations raise the question of whether displacement of the autoinhibitory glutamate is the sole mode of regulation of glutamate-containing AMPylating FIC proteins, and call for investigation of diffusible signals directly able to release autoinhibition in glutamate-bearing AMPylating FIC proteins and to regulate deAMPylation in FICD.

In this study, we addressed this question by combining structural analysis and PTM assays of a single-domain FIC protein from *Enterococcus faecalis* (EfFIC), which carries an autoinhibitory glutamate in C-terminus, and of human FICD. Enteroccoci are commensals of the gastrointestinal tract that become pathogenic outside of the gut and cause difficult-to-treat infections in the hospital due to acquisition and transmission of antibiotic resistance [22,23]. We discover that EfFIC has both AMPylation and deAMPylation activities borne by the same active site. Furthermore, the conserved glutamate implements a Ca^{2+}-controlled metal switch that tunes the balance between these activities without conformational change. Finally, we show that Ca^{2+} is an inhibitor of deAMPylation of BiP by human FICD. Our findings predict that the presence of a glutamate is a signature for AMPylation/deAMPylation bifunctionality in FIC proteins from bacteria to human, and they identify metals as diffusible signals that can directly modulate the activity of glutamate-bearing FIC proteins by binding into the active site. Importantly, they suggest that FICD is an enzymatic Ca^{2+} sensor which responds to the drop in Ca^{2+} concentration, a hallmark of ER stress, with implications in diseases that ilvolve the UPR and for therapeutic strategies.

112 **Results.**
113

114 *EfFIC is an AMPylator.*

115

116 *Enterococcus faecalis* FIC belongs to class III FIC proteins, which are comprised of a single
117 FIC domain and carry an autoinhibitory glutamate in their C-terminal α-helix. We determined
118 crystal structures of unbound, phosphate-bound, AMP-bound and ATPγS-bound wild-type
119 EfFIC ($EfFIC^{WT}$) and of unbound and sulfate-bound EfFIC carrying a mutation of the
120 catalytic histidine into an alanine ($EfFIC^{H111A}$) (**Table 1 and Table S1**). These structures
121 were obtained in different space groups, yielding 32 independent copies of the EfFIC
122 monomer with various environments in the crystal. All EfFIC monomers resemble closely to
123 each other and to structures of other class III FIC proteins (**Figure 1A**). Notably, the C-
124 terminal α-helix that bears the inhibitory glutamate shows no tendency for structural
125 flexibility, even in subunits that are free of intersubunit contacts in the crystal. The glutamate
126 has the same conformation as in other glutamate-bearing FIC protein structures (**Figure 1B**)
127 and is stabilized by intramolecular interactions and, when present, by interactions with the
128 nucleotide cofactor (**Figure 1C**). Two crystal structures were obtained in co-crystallization
129 with a non-hydrolyzable ATP analog (ATPγS), for which well-defined electron density was
130 observed for the ADP moiety (**Figure S1A**). The positions of the α and β phosphates of
131 ATPγS in these structures depart markedly from those seen in ATP bound unproductively to
132 wild type NmFIC [7], or bound non-canonically to CdFIC [11] (**Figure 1D**). In contrast, they
133 superpose well to cofactors bound in a position competent for PTM transfer [7,8] (**Figure 1E**).
134 This observation prompted us to assess whether EfFIC is competent for AMPylation, using
135 autoAMPylation as a convenient proxy in the absence of a known physiological target
136 (reviewed in [20]). Using [α-^{32}P]-ATP and autoradiography to measure the formation of
137 AMPylated EfFIC (denoted $^{AMP*}EfFIC^{WT}$), we observed that $EfFIC^{WT}$ has conspicuous
138 autoAMPylation activity in the presence of Mg^{2+} (**Figure 1F**). Mutation of the inhibitory
139 glutamate into glycine (E190G) increased AMPylation, indicating that AMPylation of
140 $EfFIC^{WT}$ is not optimal (**Figure 1F**). We conclude from these experiments that wild-type
141 EfFIC has canonical features of an AMPylating FIC enzyme, and that the inhibitory glutamate
142 mitigates this activity.
143
144

145 *EfFIC is a deAMPylator in the presence of Ca^{2+}*

146

147 To gain further insight into the enzymatic properties of EfFIC, we solved the crystal structure
148 of EfFIC bound to AMP ($EfFIC^{WT}$-AMP) (**Table 1 and Table S1**). AMP superposes exactly
149 to the AMP moiety of AMPylated CDC42 in complex with the FIC2 domain of the IbpA
150 toxin [5] (**Figure 2A)**. Electron-rich density was observed next to AMP in the active site,
151 corresponding to a calcium ion present in the crystallization solution to the exclusion of all
152 other metal ions (**Figure S1B**). Ca^{2+} has 6 coordinations with distances in the expected 2.1-
153 2.9 Å range, arranged with heptahedral geometry in which one ligand, which would be
154 located opposite to one phosphate oxygen, is missing. It interacts with the phosphate of AMP,
155 with the acidic residue in the FIC motif (Glu115), and with the inhibitory glutamate (Glu190)
156 through a water molecule (**Figure 2B**). The position of Ca^{2+} in the $EfFIC^{WT}$-AMP structure
157 differs from that of Mg^{2+} observed in other FIC protein structures in complex with ATP
158 (**Figure 2C**), raising the intriguing issue that it may have an alternative catalytic function.
159 Inspired by the recent observation that animal FICD proteins have deAMPylation enzymatic
160 activity [18,24], we analyzed whether EfFIC would have deAMPylation activity in the presence
161 of Ca^{2+}. Remarkably, addition of Ca^{2+} to $EfFIC^{WT}$ that had been previously autoAMPylated in
162 the presence of Mg^{2+} and [α-^{32}P]-ATP induced conspicuous deAMPylation (**Figure 2D**).

163

164 In the above setup, the AMPylation and deAMPylation activities are potentially acting
165 concurrently. To characterize the deAMPylation reaction selectively, the hyperactive
166 $EfFIC^{E190G}$ mutant was autoAMPylated in the presence of Mg^{2+}, purified to remove ATP, PPi
167 and Mg^{2+} such that no AMPylation remains possible, then its deAMPylation was triggered by
168 addition of $EfFIC^{WT}$ or EfFIC mutants in the presence of Ca^{2+}. The level of AMPylated EfFIC
169 (denoted $^{AMP\text{-}FAM}$EfFIC) was quantified by fluorescence using ATP-FAM, an ATP analog
170 fluorescently labeled on the adenine base. Robust deAMPylation was observed upon addition
171 of $EfFIC^{WT}$ and Ca^{2+} (**Figure 2E**, $EfFIC^{WT}$ panel). No spontaneous deAMPylation of $^{AMP\text{-}}$
172 $^{FAM}EfFIC^{E190G}$ was observed in the absence of $EfFIC^{WT}$ (**Figure 2E**, control panel), indicating
173 that the deAMPylation reaction occurs in trans. We used this deAMPylation setup to identify
174 residues critical for deAMPylation (**Figure 2E**, mutant panels). Mutation of the catalytic
175 histidine (H111A) and of the metal-binding acidic residue in the FIC motif (E115A) impaired
176 deAMPylation of $^{AMP\text{-}FAM}EfFIC^{E190G}$. Likewise, $EfFIC^{E190G}$, which carries the mutation of the
177 inhibitory glutamate, was unable to catalyze deAMPylation, consistent with the absence of
178 spontaneous deAMPylation in the assay. We conclude from these experiments that EfFIC is a

179 bifunctional enzyme, that AMPylation and deAMPylation are borne by the same active site,
180 and that the inhibitory glutamate is involved in the deAMPylation reaction.
181
182 *The AMPylation and deAMPylation reactions are differentially regulated by metals.*
183
184 The above results raise the issue of the nature of signals acting on the bifunctional active site
185 of EfFIC to regulate AMPylation/deAMPylation alternation. Previous work showed that
186 AMPylation of *Escherichia coli* DNA gyrase by NmFIC, which shares 56% sequence identity
187 with EfFIC, was highly sensitive to the toxin concentration, with a sharp drop of activity
188 above 250 μM [21]. We used purified $^{AMP\text{-}FAM}EfFIC^{E190G}$ to analyze whether the deAMPylation
189 activity of $EfFIC^{WT}$ would be similarly inhibited by increasing concentrations of $EfFIC^{WT}$ (1-
190 2000 nM). As shown in **Figure 3A**, deAMPylation increased with $EfFIC^{WT}$ concentration,
191 indicating that this reaction is not adversely affected by EfFIC concentration. Alternatively,
192 we reasoned that the distinct electrochemical properties of Ca^{2+} and Mg^{2+} (reviewed in [25])
193 may allow them to support AMPylation and deAMPylation differentially. Remarkably, Ca^{2+}
194 was unable to support AMPylation, contrary to Mg^{2+} (**Figure 3B**). In contrast, both Mg^{2+} and
195 Ca^{2+} supported potent deAMPylation (**Figure 3C, left panel**). Importantly, mutation of the
196 inhibitory glutamate eliminated the ability of EfFIC to use Ca^{2+} for deAMPylation, while the
197 mutant retained partial deAMPylation in the presence of Mg^{2+} (**Figure 3C, right panel**). To
198 understand how Ca^{2+} affects AMPylation and deAMPylation differentially, we determined the
199 crystal structure of $EfFIC^{WT}$-ATPγS-Ca^{2+}. In this structure, Ca^{2+} is heptacoordinated to the α-
200 and β-phosphates of ATPγS (of which again only the ADP moiety is visible), to the inhibitory
201 glutamate and to 4 water molecules (**Figure 3D**). Strikingly, Ca^{2+} is shifted by 3.2 Å from
202 Mg^{2+} bound to NmFIC in an equivalent configuration [7] (**Figure 3E**) and it lacks an interaction
203 with the acidic residue from the FIC motif, which explains why it inhibits AMPylation.
204 Together, these observations point towards a 3-position metal switch differentially operated
205 by Mg^{2+} and Ca^{2+}, which includes a position competent for AMPylation, a position that
206 inhibits AMPylation and a position competent for deAMPylation. To test this hypothesis, we
207 measured the apparent AMPylation efficiency of $EfFIC^{WT}$ at different Mg^{2+}/Ca^{2+} ratio. As
208 shown in **Figure 3F**, AMPylation is prominent when Mg^{2+} exceeds Ca^{2+}, while Ca^{2+} in excess
209 over Mg^{2+} favors deAMPylation. We conclude from these experiments that competition
210 between Mg^{2+} and Ca^{2+} regulates the balance between AMPylation and deAMPylation
211 efficiencies and that this regulatory metal switch is implemented by differential usage of the
212 inhibitory glutamate and the acidic residue in the FIC motif for binding metals.

213

214 *Ca^{2+} tunes deAMPylation of the BiP chaperone by human FICD.*

215

216 DeAMPylation of the BiP chaperone has been recently identified as the primary in vitro
217 activity of human FICD [18], which features a glutamate structurally equivalent to the inhibitory
218 glutamate in EfFIC (see **Figure 1B**, [10]) that is critical for deAMPylation [18]. We analyzed
219 whether, as observed in EfFIC, Mg^{2+} and Ca^{2+} metals could also affect FICD activity, using
220 fluorescent ATP-FAM to monitor BiP AMPylation. No measurable AMPylation of BiP by
221 $FICD^{WT}$ was observed, neither with Mg^{2+} nor Ca^{2+}, although $FICD^{WT}$ itself showed weak
222 autoAMPylation in the presence of both metals (**Figure 4A**). Alternatively, we used
223 $FICD^{E234G}$, in which the conserved glutamate is mutated to glycine, to produce AMPylated
224 BiP. Remarkably, while purified $^{AMP\text{-}FAM}$BIP was efficiently deAMPylated by $FICD^{WT}$ in the
225 presence of Mg^{2+}, no deAMPylation was measured in the presence of Ca^{2+} (**Figure 4B**). To
226 determine whether FICD does not bind Ca^{2+} or is unable to use it for deAMPylation, we
227 carried out an Mg^{2+}/Ca^{2+} competition experiment in which $FICD^{WT}$ and purified $^{AMP\text{-}FAM}$BiP
228 were incubated at increasing Ca^{2+} concentration and a fixed Mg^{2+} concentration. As shown in
229 **Figure 4C**, deAMPylation efficiency decreased as the Ca^{2+}/Mg^{2+} ratio increased, suggesting
230 that Ca^{2+} inhibits deAMPylation by competing with Mg^{2+}. We conclude from these
231 experiments that Ca^{2+} binds to FICD in an inhibitory manner, which allows it to tune the
232 deAMPylation efficiency of FICD towards the BiP chaperone.

233

234 **Discussion**

235

236 In this study, we sought after a diffusible signal able to regulate directly the large group of
237 AMPylating FIC proteins in which the AMPylation activity is repressed by a conserved
238 glutamate within the active site. Combining crystallography and PTM assays, we first show
239 that bacterial EfFIC is a bifunctional enzyme that encodes AMPylating and deAMPylating
240 activities and that both reactions use the same active site. Next, we discover that the balance
241 between these opposing activities is controlled by a metal switch, in which each reaction is
242 differentially supported and inhibited by Mg^{2+} and Ca^{2+} in a manner that the Mg^{2+}/Ca^{2+} ratio
243 determines the net AMPylation level. Furthermore, we identify the inhibitory glutamate and
244 the acidic residue in the FIC motif as residues essential for the metal switch. Finally, we show

that deAMPylation of the endoplasmic reticulum BiP chaperone by human FICD is also dependent on the Ca^{2+}/Mg^{2+} ratio, with high Ca^{2+} concentration inhibiting deAMPylation.

The identification of a potent deAMPylation activity in a bacterial FIC protein (this study) and in human FICD [18], which depends on a structurally equivalent glutamate in these otherwise remotely related FIC proteins, leads us to propose that the conserved glutamate is a signature of the ability of FIC proteins to catalyze both AMPylation and deAMPylation. Our data allow to delineate the catalytic basis for this bifunctionality, in which catalytic residues are shared by the AMPylation and deAMPylation reactions but have different roles in catalysis. In the AMPylation reaction, the invariant histidine in the FIC motif activates the acceptor hydroxyl of a target protein by attracting a proton and the acidic residue (Asp or Glu) in the FIC motif binds a metal that stabilizes the phosphates of the ATP cofactor at the transition state (reviewed in [2,3]). Based on the observations that the α- and β-phosphates of ATP bind with canonical positions in wild-type EfFIC and that AMPylation is potentiated by mutation of the glutamate in various FIC proteins, we propose that the primary role of the glutamate in AMPylation is to mitigate the efficiency of this reaction in the presence of Mg^{2+}, rather than to fully repress it, possibly in order to match AMPylation and deAMPylation efficiencies. In the deAMPylation mechanism depicted in **Figure 5** (see also discussion in **Supplementary data and Figure S2**), the conserved glutamate activates a water molecule for nucleophilic attack of the phosphorus of the AMP moiety, and the invariant histidine generates the free hydroxyl group in the protein residue by giving up a proton, as also proposed in [18]. The nucleophilic water molecule is readily identified as the missing ligand in the coordination sphere of Ca^{2+} in our EfFIC-AMP-Ca^{2+} structure, where it would be precisely positioned for in-line nucleophilic attack (**see Figure 2B**). Interestingly, the metal is bound to both the acidic residue of the FIC motif and the conserved glutamate in this structure, which positions it to stabilize negative charges in the AMPylated substrate that develop at the transition state.

Importantly, our data identify for the first time a diffusible signal able to modulate the activity of glutamate-bearing FIC proteins. A remarkable feature in the above bifunctional mechanism is that both reactions can be adversely regulated by a second metal that competes with the catalytic metal. In EfFIC, we observed that Ca^{2+} binds to ATP in a position that is shifted with respect to the canonical AMPylation Mg^{2+}-binding site, resulting in decreased AMPylation. In a related scenario, Ca^{2+} competes with Mg^{2+} in the deAMPylation reaction catalyzed by

279 FICD, thereby decreasing deAMPylation. This multi-position metal switch constitutes a new
280 paradigm in bifunctional enzyme regulation, in which the relative affinities of specific metals
281 for the AMPylation and deAMPylation configurations tip the balance towards opposing
282 activities within the same active site. Future studies are now needed to determine the
283 bifunctionality spectrum of glutamate-bearing FIC proteins resulting from variations in metal
284 specificities and affinities. In addition, observations by us and others that FICD has distinct
285 AMPylation and deAMPylation patterns towards itself and BiP suggests that the protein
286 substrate influences the AMPylation/deAMPylation balance through still unknown
287 mechanisms, which will have to be investigated. Another important question for future studies
288 is how other levels of regulation, such as autoAMPylations and changes in oligomerization
289 that have been described for a close homolog of EfFIC [21], combine with the intrinsic metal
290 switch identified in this study.
291
292 Our findings predict that bacterial glutamate-containing FIC proteins are bifunctional
293 enzymes able to switch between AMPylation and deAMPylation activities upon changes in
294 metal homeostasis. An appealing hypothesis is thus that glutamate-bearing FIC proteins
295 function as toxin/antitoxin (TA) modules, in which the toxin and antitoxin activities would be
296 encoded within the same active site under the control of regulatory metals. They would
297 therefore differ from type III TA modules, in which the toxin is repressed by direct interaction
298 with the antitoxin, or type IV TA modules, in which the effects of the toxin are reverted by
299 the antitoxin without direct interaction (reviewed in [26]). It is interesting to note that the
300 antitoxin component of TA modules such as Bartonella VbhT/VbhA features a structurally
301 equivalent glutamate that points into the catalytic site of the toxin [7], raising the question of
302 whether there may exist conditions where the antitoxin glutamate implements deAMPylation
303 within the TA complex. The physiological conditions that involve variations in metals
304 homeostasis to activate the switch between opposing activities in these FIC proteins, and how
305 individual bacteria exploit the bifunctionality of their FIC proteins within their ecological
306 niche or in infections will be important issues to address in future studies.
307
308 Finally, our discovery that deAMPylation of the BiP chaperone by human FICD is modulated
309 by changes in Ca^{2+} concentration raises important questions with respect to the regulation and
310 role of FICD in endoplasmic reticulum (ER) functions. The ER is the major organelle
311 involved in Ca^{2+} homeostasis (reviewed in [27-29]), and the total Ca^{2+} concentration in the ER is
312 as high as 2-3 mM under resting conditions [30]. Disruption of Ca^{2+} homeostasis, such as

313 depletion of the ER Ca^{2+} store induced by the drug thapsigargin, swiftly alters protein folding
314 processes and activates the unfolded protein response [31]. Large Ca^{2+} fluctuations are therefore
315 considered as major determinants of ER stress responses (reviewed in [28,29]). On the other
316 hand, there is currently no evidence that the Mg^{2+} concentration changes significantly in the
317 ER over time (reviewed in [32]). Thus, while keeping in mind that Ca^{2+} and Mg^{2+} concentrations
318 and local gradients in the ER have remained difficult to determine with accuracy, an
319 essentially constant Mg^{2+} concentration and Ca^{2+} fluctuations in the 10µM-3mM range, such
320 as those used in our vitro assays, are plausibly encountered in the ER as it experiences
321 transition from resting to stress conditions. Recently, FICD has been demonstrated to
322 stimulate the activity of the BiP chaperone in response to an increase in the unfolded protein
323 load [13-15,24], and this activation was correlated to deAMPylation of BiP by FICD [18]. It is thus
324 tempting to speculate that inhibition of FICD deAMPylation activity by high Ca^{2+}, which we
325 observe *in vitro*, reflects its inhibition under ER homeostasis, where Ca^{2+} concentration is
326 high and BiP activity is low. Conversely, depletion of Ca^{2+} induces ER stress and triggers the
327 UPR. Depletion of Ca^{2+} may thus release inhibition of FICD deAMPylation activity, leading
328 to efficient deAMPylation of BiP and up-regulation of its activity, which is a key feature of
329 the UPR. We propose that FICD is has features of an enzymatic sensor of Ca^{2+} in the ER,
330 which could allow it to function as an integrator between Ca^{2+} homeostasis in the ER and the
331 BiP-mediated unfolded protein response.
332
333 In conclusion, we have identified Ca^{2+} as a diffusable signal that modulates the intrinsic
334 enzymatic activity of glutamate-bearing FIC proteins directly and tips the balance between
335 AMPylation and deAMPylation reactions without a conformational change in the enzyme.
336 Future studies are now needed to investigate how the metal switch of glutamate-bearing FIC
337 protein activities is exploited in bacterial stress, and, in the case of animal FICD, its role in the
338 unfolded protein response and its crosstalks with Ca^{2+}-controled processes in the ER. The
339 detrimental effects of prolonged UPR in a myriad of diseases (reviewed in [33,34]) makes new
340 druggable targets highly desirable (reviewed in [35]). Given the established pivotal role of the
341 BiP chaperone (reviewed in [16]) and of calcium (reviewed in [29]) in this process, the Ca^{2+}-
342 regulated activity of FICD uncovered in this study may constitute a new druggable target.
343

344 **Figure Legends**

345

346 **Figure 1 : Structural basis for the AMPylation activty of EfFIC**

347 A : Structure of the EfFIC monomer showing the FIC motif (pink), the C-terminal α-helix
348 bearing the inhibitory glutamate (orange) and the β-hairpin predicted to bind protein
349 substrates (cyan). The ADP moiety of ATPγS is shown in sticks.

350 B : The inhibitory glutamate from $EfFIC^{WT}$ (orange) is structurally equivalent to the
351 glutamate found in the C-terminus of NmFIC ([7], PDB 2G03) and in the N-terminus of
352 *Bacteroides* BtFIC (PDB 3CUC), *Clostridium* CdFIC ([11], PDB 4X2E) and of human
353 FICD/HYPE ([10], PDB 4U04). Superpositions are done on the structurally highly conserved
354 FIC motif.

355 C : Interactions of the inhibitory glutamate with the active site of ATPγS-bound $EfFIC^{WT}$.
356 Hydrogen bonds are depicted by dotted lines.

357 D : The positions of the α- and β-phosphates of ATPγS bound to $EfFIC^{WT}$ (yellow) diverge
358 from those of ATPγS bound to $NmFIC^{WT}$ (cyan, [7], PDB 3S6A) and of ATP bound to CdFIC
359 (blue, [11], S31A/E35A mutant, PDB 4X2D) in a non-canonical conformations. Note that only
360 the ADP moiety of ATPγS is visible in the $EfFIC^{WT}$ and $NmFIC^{WT}$ crystal structures.

361 E : The α- and β-phosphates of ATPγS bound to $EfFIC^{WT}$ (yellow) superpose well to those of
362 ATP bound to NmFIC (purple, [7], E186G mutant, PDB 3ZLM) and of CDP-choline bound to
363 AnkX (green, [8], H229A mutant, PDB 4BET) in a PTM-competent conformation.

364 F : AutoAMPylation of $EfFIC^{WT}$ and $EfFIC^{E190G}$. The level of AMPylated proteins (indicated
365 as $^{AMP*}EfFIC^{WT}$) was measured by autoradiography using radioactive [α-^{32}P]-ATP in the
366 presence of 100 nM Mg^{2+}. The reaction was carried out for one hour for $EfFIC^{WT}$ and five
367 minutes for $EfFIC^{E190G}$. The total amount of $EfFIC^{WT}$ measured by Coomassie staining in the
368 same sample is shown.

369

370 **Figure 2 : EfFIC is a deAMPylator in the presence of Ca^{2+}**

371 A : AMP bound to $EfFIC^{WT}$ superposes with the AMP moiety of AMPylated CDC42 in
372 complex with the FIC protein IbpA ([5], PDB 4ITR). Superposition was carried out based on
373 the FIC motif.

374 B : Close-up view of Ca^{2+} bound to $EfFIC^{WT}$-AMP. The incomplete heptagonal coordination
375 sphere of Ca^{2+} is indicated by dotted lines. Water molecules are shown as red spheres. The

376 proposed position of the water molecule responsible for in-line nucleophilic attack is
377 indicated in grey.
378 C: Ca^{2+} bound to $EfFIC^{WT}$-AMP is shifted by 1.3 Å with respect to Mg^{2+} bound to $NmFIC^{E/G}$-
379 AMPPNP. The superposition is done on the FIC motif.
380 D : $EfFIC^{WT}$ has deAMPylation activity in the presence of Ca^{2+}. $EfFIC^{WT}$ was
381 autoAMPylated with [α-^{32}P]-ATP in the presence 100 nM Mg^{2+} for one hour, then the sample
382 was incubated for 60 minutes with EDTA alone (1mM) (lane "-") or 5, 30 and 60 minutes
383 with EDTA (1mM) and an excess of Ca^{2+} (10 mM) (lanes "+"). AMPylation levels were
384 analyzed by autoradiography (upper panel). The total amount of $EfFIC^{WT}$ in each sample was
385 measured by Coomassie staining (lower panel).
386 E : Key residues of the AMPylation active site are required for deAMPylation. $EfFIC^{E190G}$
387 was auto-AMPylated for one hour in the presence of fluorescently-labeled ATP-FAM and
388 Mg^{2+}, then $^{AMP\text{-}FAM}EfFIC^{E190G}$ was purified to remove Mg^{2+}, PPi and ATP-FAM.
389 DeAMPylation was then triggered by addition of wild-type or mutant EfFIC as indicated in
390 the presence or not of 1mM Ca^{2+}. AMPylation levels (indicated as $^{AMP\text{-}FAM}EfFIC^{E190G}$) after
391 one hour incubation were analyzed by fluorescence (upper panel). The total amount of EfFIC
392 proteins (indicated as $EfFIC^{total}$) in each sample was measured by Coomassie staining (lower
393 panel).
394
395 **Figure 3 : The Mg^{2+}/Ca^{2+} ratio tunes the balance between EfFIC AMPylation and de-**
396 **AMPylation activities**
397 A : DeAMPylation is not inhibited at high EfFIC concentration. Purified $^{AMP\text{-}FAM}EfFIC^{E190G}$
398 was incubated with increasing concentrations of $EfFIC^{WT}$ for one hour in the presence of
399 100µM Ca^{2+}. AMPylation levels were measured by fluorescence as in **Figure 2D**.
400 B : $EfFIC^{WT}$ uses Mg^{2+} but not Ca^{2+} for autoAMPylation. AutoAMPylation was carried out at
401 1mM Ca^{2+} or Mg^{2+} for one hour and was measured by autoradiography as in **Figure 1F**.
402 C : The conserved glutamate of EfFIC is required for the usage of both Mg^{2+} and Ca^{2+} for
403 deAMPylation. Experiments were carried out for one hour as in **Figure 3A** in the presence of
404 0.5mM EDTA and 3mM of Mg^{2+} or Ca^{2+}. Quantification of deAMPylation efficiencies is
405 shown on the right panel.
406 D: Close-up view of Ca^{2+} bound to $EfFIC^{WT}$-ATPγS. The heptagonal coordination sphere of
407 Ca^{2+} is indicated by dotted lines. Water molecules are shown as red spheres.

408 E : Ca^{2+} bound to $EfFIC^{WT}$-ATPγS is shifted with respect to Mg^{2+} bound to AMPylation-
409 competent $NmFIC^{E/G}$-AMPPNP (PDF 2ZLM).
410 F: The net AMPylation efficiency of $EfFIC^{WT}$ is controled by the Mg^{2+}/Ca^{2+} ratio. $EfFIC^{WT}$
411 was incubated for one hour in the presence of ATP-FAM at fixed Mg^{2+} concentration (1mM)
412 and increasing concentrations of Ca^{2+}. $^{AMP\text{-}FAM}$EfFIC levels were measured by fluorescence.
413 The steady-state AMPylation efficiency, which results from the relative AMPylation and
414 deAMPylation rates, is expressed as the percentage of the maximal AMPylation level
415 obtained with Mg^{2+} alone. All measurements have p-values <0.05 with respect to the
416 experiment containing Mg^{2+} alone. The total amount of $EfFIC^{WT}$ measured by Coomassie
417 staining in each sample is shown.
418
419 **Figure 4: DeAMPylation of BiP by FICD requires Mg^{2+} and is inhibited by Ca^{2+}.**
420 A: $FICD^{WT}$ does not AMPylate the BiP chaperone. Reactions were carried out for one hour in
421 presence of 1mM Mg^{2+} or 1mM Ca^{2+}. The level of AMPylated proteins (indicated as $^{AMP\text{-}}$
422 $^{FAM}FICD^{WT}$ and $^{AMP\text{-}FAM}$BIP) was measured by fluorescence. The total amount of proteins
423 measured by Coomassie staining in the same sample is shown.
424 B: Ca^{2+} inhibits deAMPylation of BiP by $FICD/HYPE^{WT}$. BiP was first AMPylated for one
425 hour by the hyperactive $FICD^{E234G}$ mutant in the presence of 100 μM Mg^{2+}, then $^{AMP\text{-}FAM}$BIP
426 was purified to remove Mg^{2+}, PPi and ATP-FAM. DeAMPylation of $^{AMP\text{-}FAM}$BIP was then
427 triggered by addition of wild-type or mutant FICD as indicated in the presence of 1mM Mg^{2+}
428 or 1mM Ca^{2+}. $^{AMP\text{-}FAM}$BiP levels were measured by fluorescence. The total amount of BiP
429 measured by Coomassie staining in each sample is shown.
430 C: The net deAMPylation efficiency of $FICD^{WT}$ is tuned by the Mg^{2+}/Ca^{2+} ratio.
431 DeAMPylation was carried out as in **Figure 4B** using a fixed Mg^{2+} concentration (200μM)
432 and 0, 1, 2 or 3mM Ca^{2+}. AMPylation levels were measured by fluorescence, normalized to
433 the fluorescence intensity of FICD and expressed as the percentage of maximal
434 deAMPylation level obtained in the absence of Ca^{2+}. All data have p-values <0.05 with
435 respect to the control in the absence of Ca^{2+}. The total amount of BiP measured by Coomassie
436 staining in each sample is shown.
437
438 **Figure 5: Model of the Ca^{2+}-assisted deAMPylation catalytic mechanism.**
439 In this model, the regulatory glutamate (Glu190 in EfFIC) attracts a proton from a water
440 molecule coordinating the metallic cation (1) to activate it for nucleophilic attack of its
441 oxygen on the phosphorus of AMP moiety in the AMPylated substrate (2). The positive

charge provided by Ca^{2+} increases electrophilicity of the phosphorus and stabilizes the negative charge of the intermediate (2 and 3). The intermediate harboring a pentavalent phosphorus then rearranges, leading to the breaking of the phosphor-ester bond, which is elicited by the capture of a proton provided by the catalytic histidine (4). R : AMPylated protein.

Material and Methods.

Protein cloning, expression and purification

The codon-optimized gene encoding full-length *Enterococcus faecalis* EfFIC with an N-terminal 6-histidine tag was from GeneArt Gene Synthesis (ThermoFisher Scientific) and cloned into a pET22b(+) vector. The codon-optimized gene encoding human FICD/HYPE (residues 45-459) carrying an N-terminal 6-His tag followed by SUMO tag was from GeneArt Gene Synthesis and cloned into a pET151/D-TOPO vector (ThermoFisher Scientific). All mutations were performed with the QuickChange II mutagenesis kit (Agilent). *Mus musculus* BIP in pUJ4 plasmid is a kind gift from Ronald Melki (CNRS, Gif-sur-Yvette). All constructs were verified by sequencing (GATC). All EfFIC constructs were expressed in *E. coli* BL21 (DE3) pLysS in LB medium. Overexpression was induced overnight with 0.5 mM IPTG at 20°C. Bacterial cultures were centrifuged for 40 min at 4000g. Bacterial pellets were resuspended in lysis buffer (50 mM Tris-HCl pH 8.0, 150 mM NaCl, 5% glycerol, 0.25 mg/mL lysozyme) containing a protease inhibitor cocktail, disrupted at 125 psi using a high pressure cell disrupter and centrifuged 30 min at 22000g. The cleared lysate supernatant was loaded on a Ni-NTA affinity chromatography column (HisTrap FF, GE Healthcare) and eluted with 250 mM imidazole. Purification was polished by gel filtration on a Superdex 200 16/600 column (GE Healthcare) equilibrated with storage buffer (50 mM Tris-HCl pH 8.0, 150 mM NaCl). Wild-type and mutant FICD/HYPE were expressed and purified as EfFIC, except that the lysis buffer was complemented with 1mM DTT and 0.02% Triton X-100 and other buffers with 1mM DTT. To remove the SUMO tag, FICD/HYPE was incubated with SUMO protease (ThermoFischer) at 1/100 weight/weight ratio during 1 hour at room temperature. The cleaved fraction was separated by affinity chromatography (HisTrap FF, GE Healthcare) and further purified by gel filtration on a Superdex 200 10/300 column (GE Healthcare) equilibrated with storage buffer (50 mM Tris pH 8.0, 150 mM NaCl, 1mM DTT, 5% glycerol). Mouse BIP was expressed and purified essentially as EfFIC.

476

477 *Crystallization and structure determination*

478

479 A summary of the crystal structures determined in this study is in **Table 1**. Proteins were
480 crystallized using a TTP Labtech's Mosquito LCP crystallization robot and crystallization
481 screens (Jena Bioscience and Quiagen). Conditions leading to crystals were subsequently
482 optimized. Diffraction data sets were recorded at synchrotron SOLEIL and ESRF. Datasets
483 were processed using XDS [36], xdsme (https://github.com/legrandp/xdsme) or autoProc [37].
484 Structures were solved by molecular replacement and refined with the Phenix suite [38] or
485 Buster (Bricogne G., Blanc E., Brandl M., Flensburg C., Keller P., Paciorek W.,Roversi P,
486 Sharff A., Smart O.S., Vonrhein C., Womack T.O. (2017). BUSTER version 2.10.2.
487 Cambridge, United Kingdom: Global Phasing Ltd.). Models were build using Coot [39].
488 Softwares used in this project were curated by SBGrid [40]. Crystallization conditions, data
489 collection statistics and refinement statistics are given in **Table S1**. All structures have been
490 deposited with the Protein Data Bank (PDB codes in **Table S1**).

491

492 *AMPylation and deAMPylation assays*

493

494 AMPylation and deAMPylation autoradiography assays were carried out using the following
495 protocols. For AMPylation reactions, 8 µg of purified proteins were mixed with 10 µCi [α-
496 ^{32}P] ATP (Perkin Elmer) in a buffer containing 50mM Tris-HCl pH 7.4, 150 mM NaCl and
497 0.1 mM $MgCl_2$. Reactions were incubated for 1 h at 30 °C, then stopped with reducing SDS
498 sample buffer and boiling for 5 min. For deAMPylation, AMPylation was performed as
499 above, then 1 mM EDTA was added with or without 10 mM $CaCl_2$. Proteins were resolved by
500 SDS-PAGE and AMPylation was revealed by autoradiography.
501 EfFIC AMPylation and deAMPylation fluorescence assays were carried out using the
502 following protocols. AMPylation was carried out using a fluorescent ATP analog modified by
503 N^6-(6-Amino)hexyl on the adenine base (ATP-FAM, Jena Bioscience). AMPylated proteins
504 were obtained by incubation for one hour at 30 °C in 50mM Tris pH 8.0, 150 mM NaCl,
505 0.1 mM $MgCl_2$ and an equimolar amount of ATP-FAM. Before deAMPylation reactions, the
506 buffer was exchanged to 50 mM Tris-HCl pH 8.0 and 150 mM NaCl by 5 cycles of
507 dilution/concentration on a Vivaspin-500 with a cut-off of 10kDa (Sartorius), resulting in a
508 final dilution of ATP-FAM, $MgCl_2$ and PPi by about 10^5 times. DeAMPylation reactions
509 were carried out using 3 µM of AMPylated protein and 6 µM of freshly purified EfFIC

510 proteins (except for the experiment depicted in Figure 3A) in a buffer containing 50mM Tris-
511 HCl pH 8.0 and 150 mM NaCl, for 1h at 30°C. Reactions were stopped by addition of
512 reducing SDS sample buffer and boiling for 5 min. Proteins were resolved by SDS-PAGE and
513 modification by AMP-FAM was revealed by fluorescence using green channel (excitation:
514 488 nm, emission: 526 nm) on a Chemidoc XR+ Imaging System (BioRad).
515 FICD AMPylation and deAMPylation fluorescence assays were carried out using the
516 following protocols. AMPylation was carried out using fluorescent ATP-FAM. AMPylated
517 BIP was obtained by incubation for one hour at 30 °C in 50mM Tris pH 8.0, 150 mM NaCl,
518 0.1 mM $MgCl_2$, 2µM $FICD^{E234G}$ and an equimolar amount of ATP-FAM. Before
519 deAMPylation reactions, the buffer was exchanged with 50mM Tris-HCl pH 8.0 and 150 mM
520 NaCl by 5 cycles of dilution/concentration on a Vivaspin-500 with a cut-off of 50kDa
521 (Sartorius), resulting in a final dilution of ATP-FAM, $MgCl_2$ and PPi produced by the
522 reaction of about 10^5 times. DeAMPylation reactions were carried using 2 µg of AMPylated
523 protein and 4 µg of freshly purified $FICD^{WT}$ in a buffer containing 50mM Tris pH 8.0 and
524 150 mM NaCl, for 1h at 30°C. Reactions were stopped and ATP-FAM modification revealed
525 as EfFIC. Quantification of AMP-FAM levels was done using (ImageLab, BioRad).
526 All experiments were done at least in triplicate, except kinetics in Figure 3A that were done in
527 duplicate.
528
529 **Acknowledgements.**
530
531 This work was supported by grants from the Fondation pour la Recherche Médicale and from
532 the Agence Nationale pour la Recherche to J.C. and by grants n°ANR-10-LABX-62-IBEID
533 and from the Fondation pour la Recherche Médicale to C.B. S.V. was supported by a PhD
534 grant from the DIM MALINF and G.O. by a stipend from the Pasteur-Paris University
535 International PhD program. We are grateful to the scientific teams at the PX1 and PX2
536 beamlines at the SOLEIL synchrotron (Gif-sur-Yvette, France) and from the ID29, ID30-A3
537 and ID30B beamlines at the European Synchrotron Research Facility (ESRF, Grenoble,
538 France) for their expertise and advice. We thank Pascale Serror (INRA, Jouy-en-Josas,
539 France) and Philippe Glaser (Institut Pasteur) for discussions and the members of the Cherfils
540 lab for help and shared expertise.
541

542 **Table 1 – Summary of crystal structures of EfFIC determined in this study**. All crystals
543 have cell angles of α, β and γ = 90°. Crystallographic statistics are given in **Table S1**. * : only
544 the ADP moiety is visible.
545

Form	Space group	Cell parameters *a*, *b*, *c* (Å)	Ligand	Resolution	PDB
WT	$P4_12_12$	65.13, 65.13, 248.06	PO_4^{2-}	2.29	6ER8
WT	I222	121.54, 131.00, 136.94	/	2.40	5NV5
WT	$P4_12_12$	64.98 64.98 246.24	AMP – Ca^{2+}	2.35	6EP0
WT	$P4_32_12$	125.35 125.35 362.8	ATPγS* – Ca^{2+}	2.15	6EP2
WT	$P4_32_12$	87.84 87.84 364.94	ATPγS*	1.93	6EP5
H118A	$P2_122_1$	76.67 77.11 103.15	/	2.60	5NWF
H118A	I222	121.93 131.16 136.71	SO_4^{2-}	2.20	5NVQ

546

547 **References**

548

549 1. Kinch, L.N., Yarbrough, M.L., Orth, K. & Grishin, N.V. Fido, a novel AMPylation
550 domain common to fic, doc, and AvrB. *PLoS One* **4**, e5818 (2009).
551 2. Garcia-Pino, A., Zenkin, N. & Loris, R. The many faces of Fic: structural and
552 functional aspects of Fic enzymes. *Trends Biochem Sci* **39**, 121-9 (2014).
553 3. Roy, C.R. & Cherfils, J. Structure and function of Fic proteins. *Nat Rev Microbiol* **13**,
554 631-40 (2015).
555 4. Harms, A., Stanger, F.V. & Dehio, C. Biological Diversity and Molecular Plasticity of
556 FIC Domain Proteins. *Annu Rev Microbiol* **70**, 341-60 (2016).
557 5. Xiao, J., Worby, C.A., Mattoo, S., Sankaran, B. & Dixon, J.E. Structural basis of Fic-
558 mediated adenylylation. *Nat Struct Mol Biol* **17**, 1004-10 (2010).
559 6. Luong, P. et al. Kinetic and structural insights into the mechanism of AMPylation by
560 VopS Fic domain. *J Biol Chem* **285**, 20155-63 (2010).
561 7. Engel, P. et al. Adenylylation control by intra- or intermolecular active-site
562 obstruction in Fic proteins. *Nature* **482**, 107-10 (2012).
563 8. Campanacci, V., Mukherjee, S., Roy, C.R. & Cherfils, J. Structure of the Legionella
564 effector AnkX reveals the mechanism of phosphocholine transfer by the FIC domain.
565 *EMBO J* **32**, 1469-77 (2013).
566 9. Castro-Roa, D. et al. The Fic protein Doc uses an inverted substrate to phosphorylate
567 and inactivate EF-Tu. *Nat Chem Biol* **9**, 811-7 (2013).
568 10. Bunney, T.D. et al. Crystal structure of the human, FIC-domain containing protein
569 HYPE and implications for its functions. *Structure* **22**, 1831-43 (2014).
570 11. Dedic, E. et al. A Novel Fic (Filamentation Induced by cAMP) Protein from
571 Clostridium difficile Reveals an Inhibitory Motif-independent
572 Adenylylation/AMPylation Mechanism. *J Biol Chem* **291**, 13286-300 (2016).
573 12. Yarbrough, M.L. et al. AMPylation of Rho GTPases by Vibrio VopS disrupts effector
574 binding and downstream signaling. *Science* **323**, 269-72 (2009).
575 13. Sanyal, A. et al. A novel link between Fic (filamentation induced by cAMP)-mediated
576 adenylylation/AMPylation and the unfolded protein response. *J Biol Chem* **290**, 8482-
577 99 (2015).
578 14. Ham, H. et al. Unfolded protein response-regulated Drosophila Fic (dFic) protein
579 reversibly AMPylates BiP chaperone during endoplasmic reticulum homeostasis. *J*
580 *Biol Chem* **289**, 36059-69 (2014).

581 15. Preissler, S. et al. AMPylation matches BiP activity to client protein load in the
582 endoplasmic reticulum. *Elife* **4**, e12621 (2015).
583 16. Zhao, L. & Ackerman, S.L. Endoplasmic reticulum stress in health and disease. *Curr*
584 *Opin Cell Biol* **18**, 444-52 (2006).
585 17. Preissler, S. et al. AMPylation targets the rate-limiting step of BiP's ATPase cycle for
586 its functional inactivation. *Elife* **6**(2017).
587 18. Preissler, S., Rato, C., Perera, L.A., Saudek, V. & Ron, D. FICD acts bifunctionally to
588 AMPylate and de-AMPylate the endoplasmic reticulum chaperone BiP. *Nat Struct*
589 *Mol Biol* **24**, 23-29 (2017).
590 19. Das, D. et al. Crystal structure of the Fic (Filamentation induced by cAMP) family
591 protein SO4266 (gi|24375750) from Shewanella oneidensis MR-1 at 1.6 A resolution.
592 *Proteins* **75**, 264-71 (2009).
593 20. Veyron, S., Peyroche, G. & Cherfils, J. FIC proteins: from bacteria to humans and
594 back again. *Pathog Dis* **76**(2018).
595 21. Stanger, F.V. et al. Intrinsic regulation of FIC-domain AMP-transferases by
596 oligomerization and automodification. *Proc Natl Acad Sci U S A* **113**, E529-37 (2016).
597 22. Hegstad, K., Mikalsen, T., Coque, T.M., Werner, G. & Sundsfjord, A. Mobile genetic
598 elements and their contribution to the emergence of antimicrobial resistant
599 Enterococcus faecalis and Enterococcus faecium. *Clin Microbiol Infect* **16**, 541-54
600 (2010).
601 23. Lebreton, F. et al. Tracing the Enterococci from Paleozoic Origins to the Hospital.
602 *Cell* **169**, 849-861 e13 (2017).
603 24. Casey, A.K. et al. Fic-mediated deAMPylation is not dependent on homodimerization
604 and rescues toxic AMPylation in flies. *J Biol Chem* **292**, 21193-21204 (2017).
605 25. Carafoli, E. & Krebs, J. Why Calcium? How Calcium Became the Best
606 Communicator. *J Biol Chem* **291**, 20849-20857 (2016).
607 26. Harms, A., Brodersen, D.E., Mitarai, N. & Gerdes, K. Toxins, Targets, and Triggers:
608 An Overview of Toxin-Antitoxin Biology. *Mol Cell* **70**, 768-784 (2018).
609 27. Bravo, R. et al. Endoplasmic reticulum and the unfolded protein response: dynamics
610 and metabolic integration. *Int Rev Cell Mol Biol* **301**, 215-90 (2013).
611 28. Krebs, J., Agellon, L.B. & Michalak, M. Ca(2+) homeostasis and endoplasmic
612 reticulum (ER) stress: An integrated view of calcium signaling. *Biochem Biophys Res*
613 *Commun* **460**, 114-21 (2015).

614 29. Carreras-Sureda, A., Pihan, P. & Hetz, C. Calcium signaling at the endoplasmic
615 reticulum: fine-tuning stress responses. *Cell Calcium* **70**, 24-31 (2018).
616 30. Montero, M. et al. Monitoring dynamic changes in free Ca2+ concentration in the
617 endoplasmic reticulum of intact cells. *EMBO J* **14**, 5467-75 (1995).
618 31. Wong, W.L., Brostrom, M.A., Kuznetsov, G., Gmitter-Yellen, D. & Brostrom, C.O.
619 Inhibition of protein synthesis and early protein processing by thapsigargin in cultured
620 cells. *Biochem J* **289 (Pt 1)**, 71-9 (1993).
621 32. Romani, A.M. Cellular magnesium homeostasis. *Arch Biochem Biophys* **512**, 1-23
622 (2011).
623 33. Xu, C., Bailly-Maitre, B. & Reed, J.C. Endoplasmic reticulum stress: cell life and
624 death decisions. *J Clin Invest* **115**, 2656-64 (2005).
625 34. Morris, G. et al. The Endoplasmic Reticulum Stress Response in Neuroprogressive
626 Diseases: Emerging Pathophysiological Role and Translational Implications. *Mol*
627 *Neurobiol* (2018).
628 35. Maly, D.J. & Papa, F.R. Druggable sensors of the unfolded protein response. *Nat*
629 *Chem Biol* **10**, 892-901 (2014).
630 36. Kabsch, W. Integration, scaling, space-group assignment and post-refinement. *Acta*
631 *Crystallogr D Biol Crystallogr* **66**, 133-44 (2010).
632 37. Vonrhein, C. et al. Data processing and analysis with the autoPROC toolbox. *Acta*
633 *Crystallogr D Biol Crystallogr* **67**, 293-302 (2011).
634 38. Adams, P.D. et al. PHENIX: a comprehensive Python-based system for
635 macromolecular structure solution. *Acta Crystallogr D Biol Crystallogr* **66**, 213-21
636 (2010).
637 39. Emsley, P. & Cowtan, K. Coot: model-building tools for molecular graphics. *Acta*
638 *crystallographica. Section D, Biological crystallography* **60**, 2126-32 (2004).
639 40. Morin, A. et al. Collaboration gets the most out of software. *Elife* **2**, e01456 (2013).
640

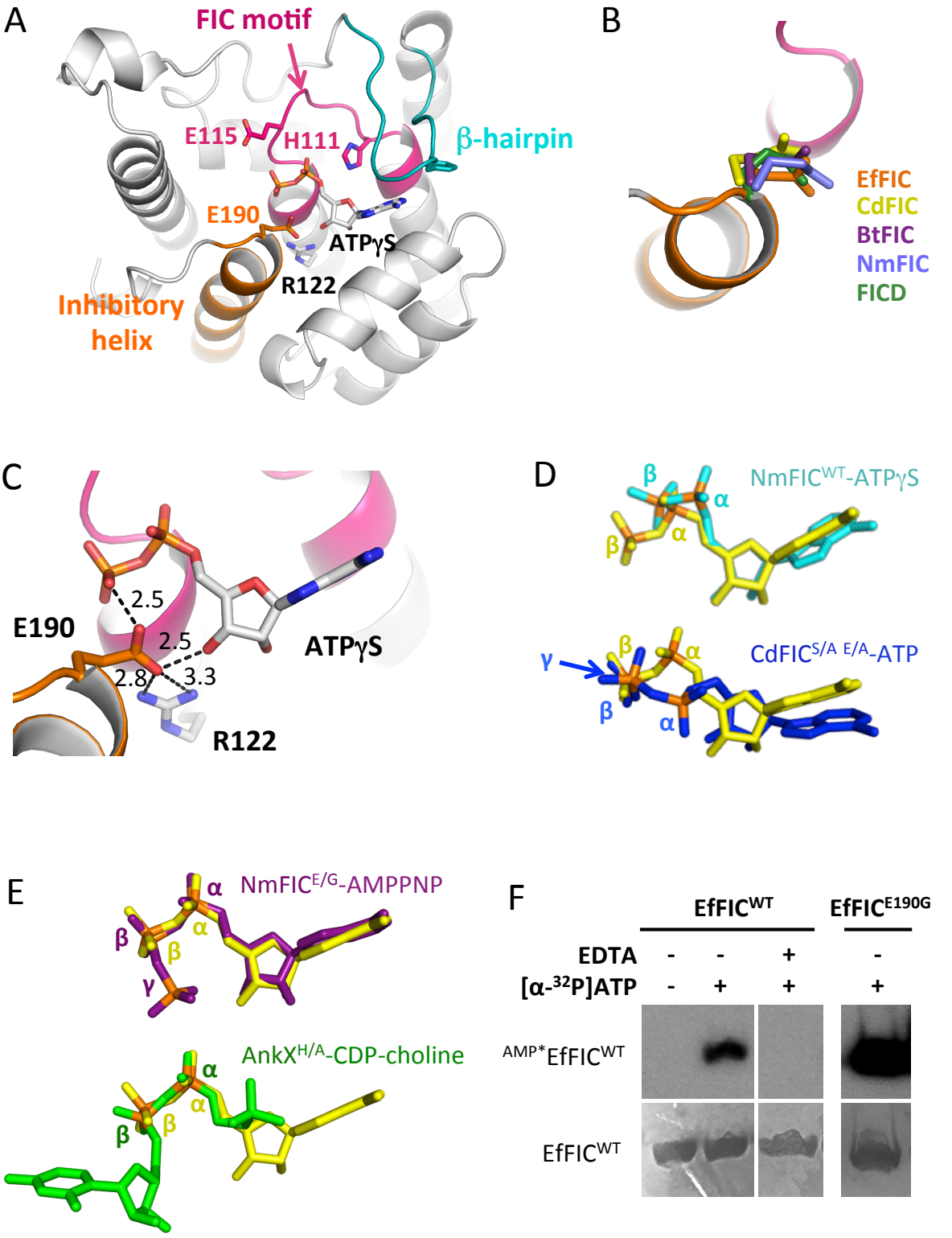
A
FIC motif
E115
H111
β-hairpin
E190
ATPγS
R122
Inhibitory helix
B
EfFIC
CdFIC
BtFIC
NmFIC
FICD
C
2.5
E190
2.5
ATPγS
2.8
3.3
R122
D
NmFIC^WT-ATPγS
CdFIC^S/A E/A-ATP
E
NmFIC^E/G-AMPPNP
AnkX^H/A-CDP-choline
F
EfFIC^WT
EfFIC^E190G
EDTA
[α-32P]ATP
AMP*EfFIC^WT
EfFIC^WT

Figure 1

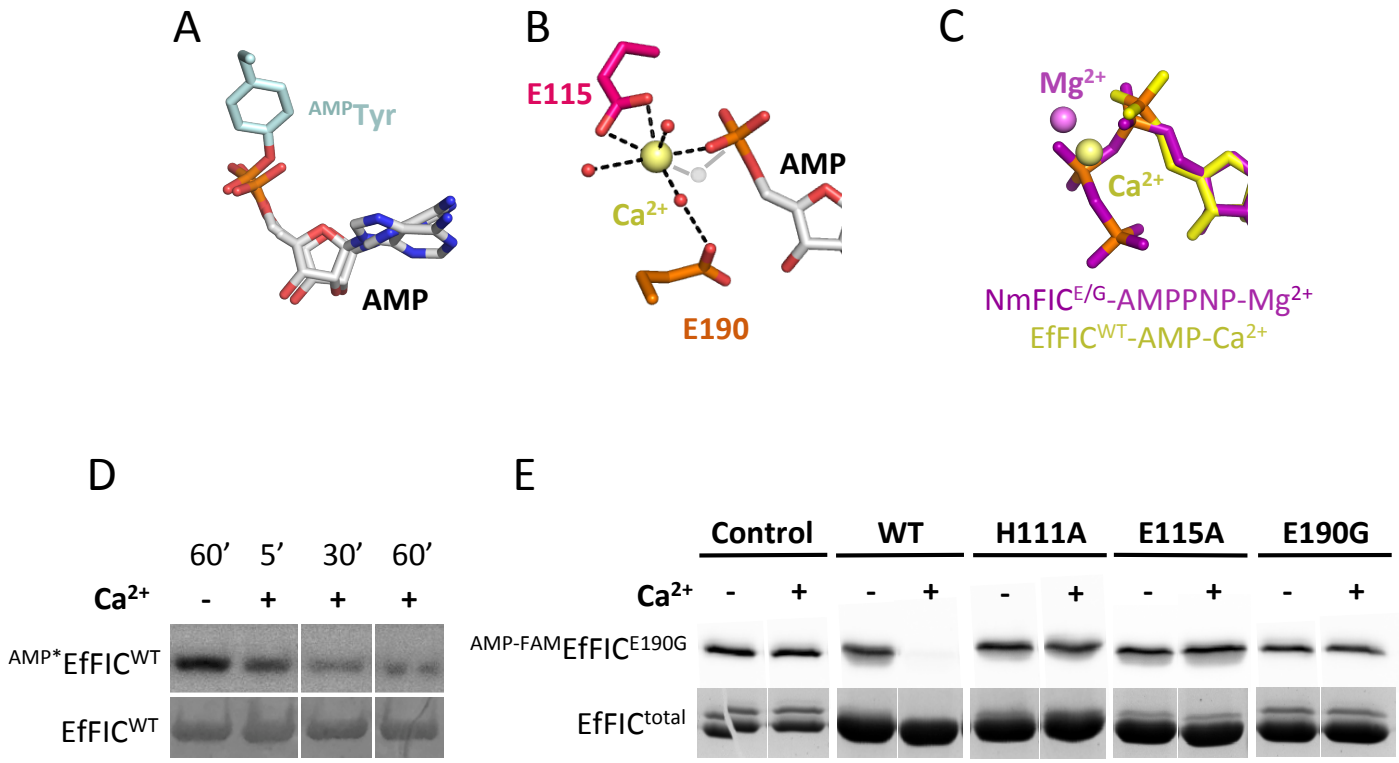
A
AMPTyr
AMP
B
E115
AMP
Ca2+
E190
C
Mg2+
Ca2+
NmFICE/G-AMPPNP-Mg2+
EfFICWT-AMP-Ca2+
D
60' 5' 30' 60'
Ca2+ - + + +
AMP*EfFICWT
EfFICWT
E
Control WT H111A E115A E190G
Ca2+ - + - + - + - + - +
AMP-FAMEfFICE190G
EfFICtotal

Figure 2

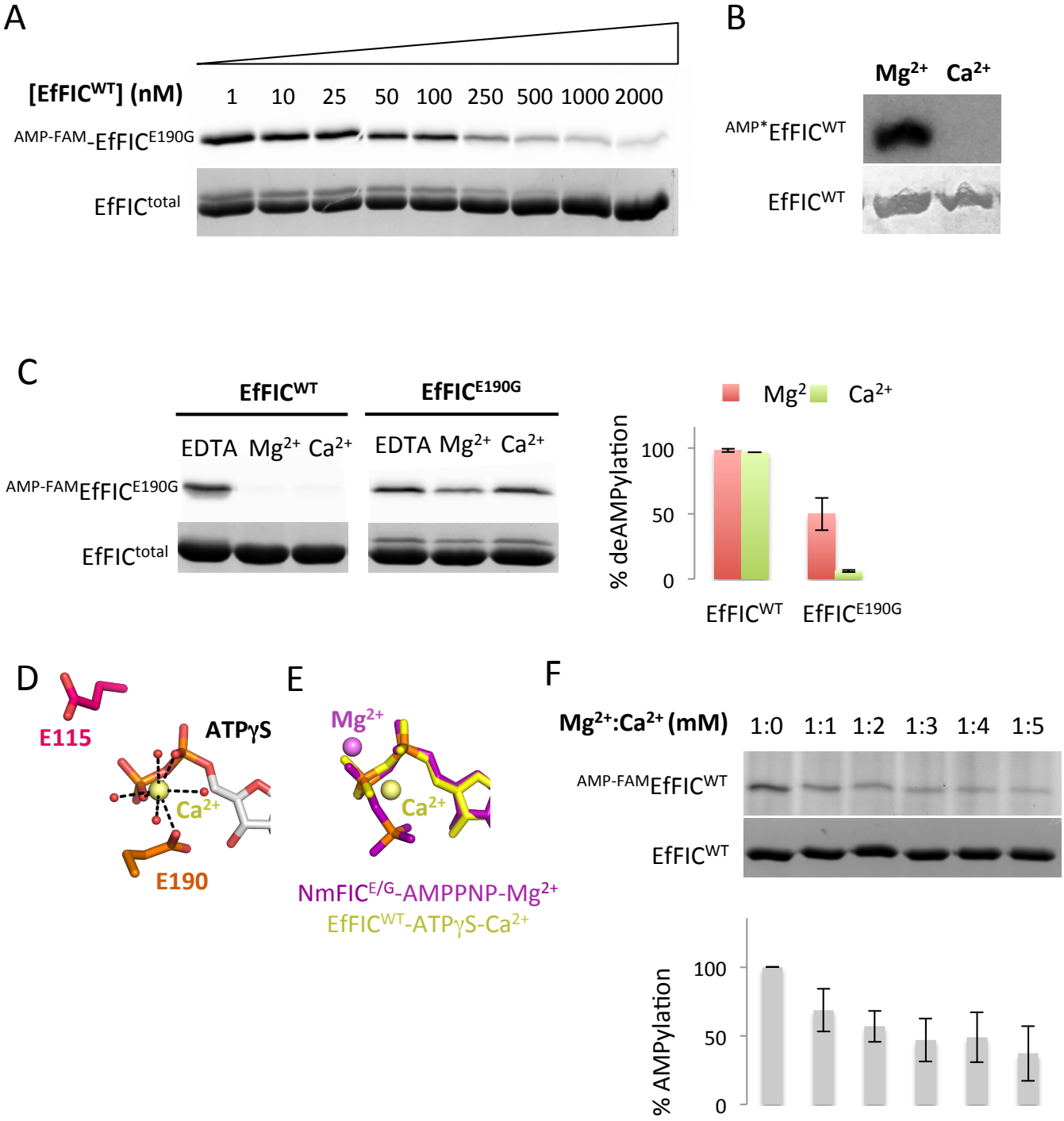
A
[EfFIC^WT] (nM)
1 10 25 50 100 250 500 1000 2000
AMP-FAM-EfFIC^E190G
EfFIC^total
B
Mg2+ Ca2+
AMP*EfFIC^WT
EfFIC^WT
C
EfFIC^WT
EfFIC^E190G
EDTA Mg2+ Ca2+
EDTA Mg2+ Ca2+
AMP-FAMEfFIC^E190G
EfFIC^total
Mg2 Ca2+
% deAMPylation
100
50
0
EfFIC^WT EfFIC^E190G
D
E115
ATPγS
Ca2+
E190
E
Mg2+
Ca2+
NmFIC^E/G-AMPPNP-Mg2+
EfFIC^WT-ATPγS-Ca2+
F
Mg2+:Ca2+ (mM)
1:0 1:1 1:2 1:3 1:4 1:5
AMP-FAMEfFIC^WT
EfFIC^WT
% AMPylation
100
50
0

Figure 3

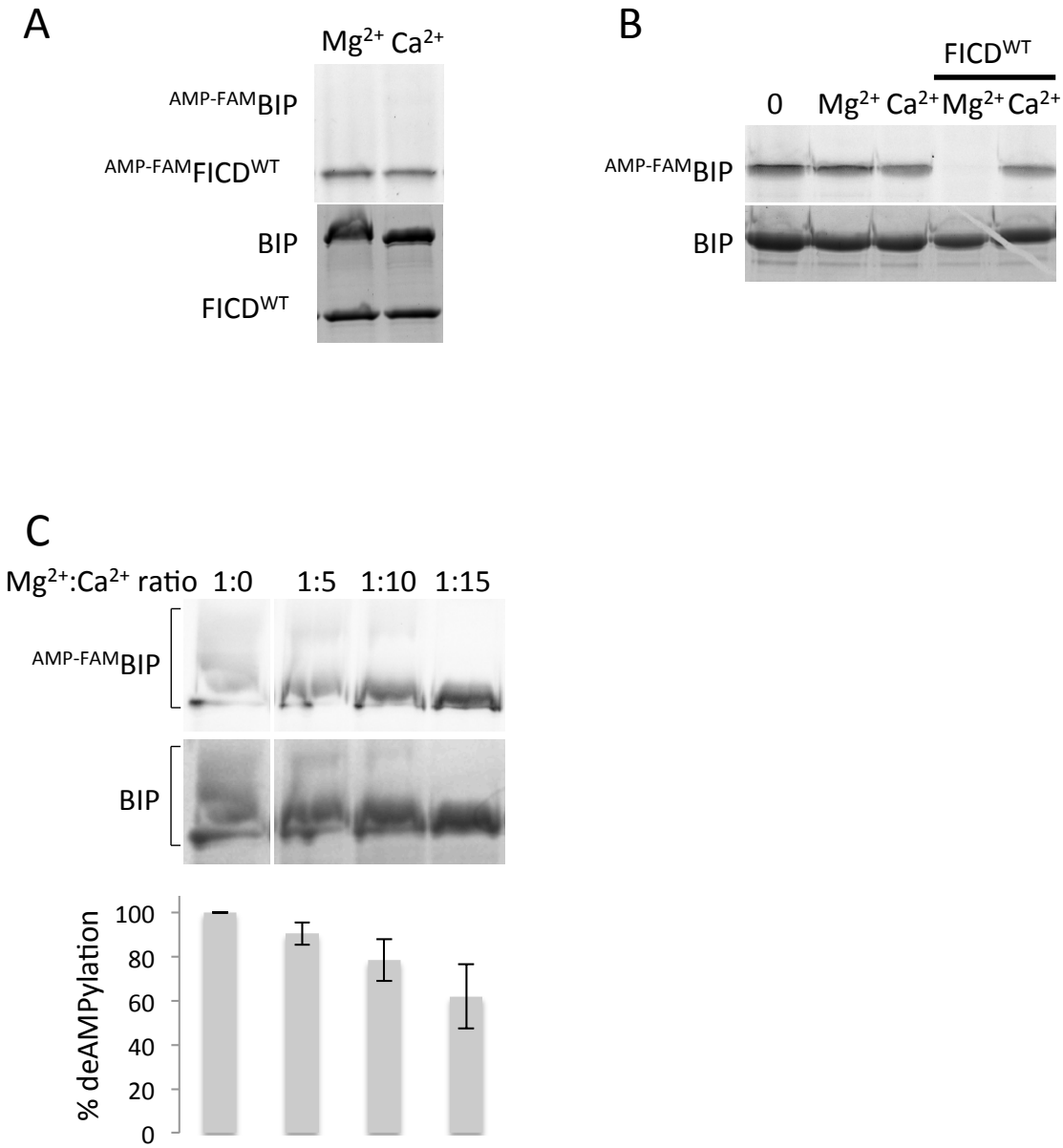
A
Mg2+ Ca2+
AMP-FAMBIP
AMP-FAMFICDWT
BIP
FICDWT
B
FICDWT
0 Mg2+ Ca2+ Mg2+ Ca2+
AMP-FAMBIP
BIP
C
Mg2+:Ca2+ ratio 1:0 1:5 1:10 1:15
AMP-FAMBIP
BIP
% deAMPylation
100
80
60
40
20
0

Figure 4

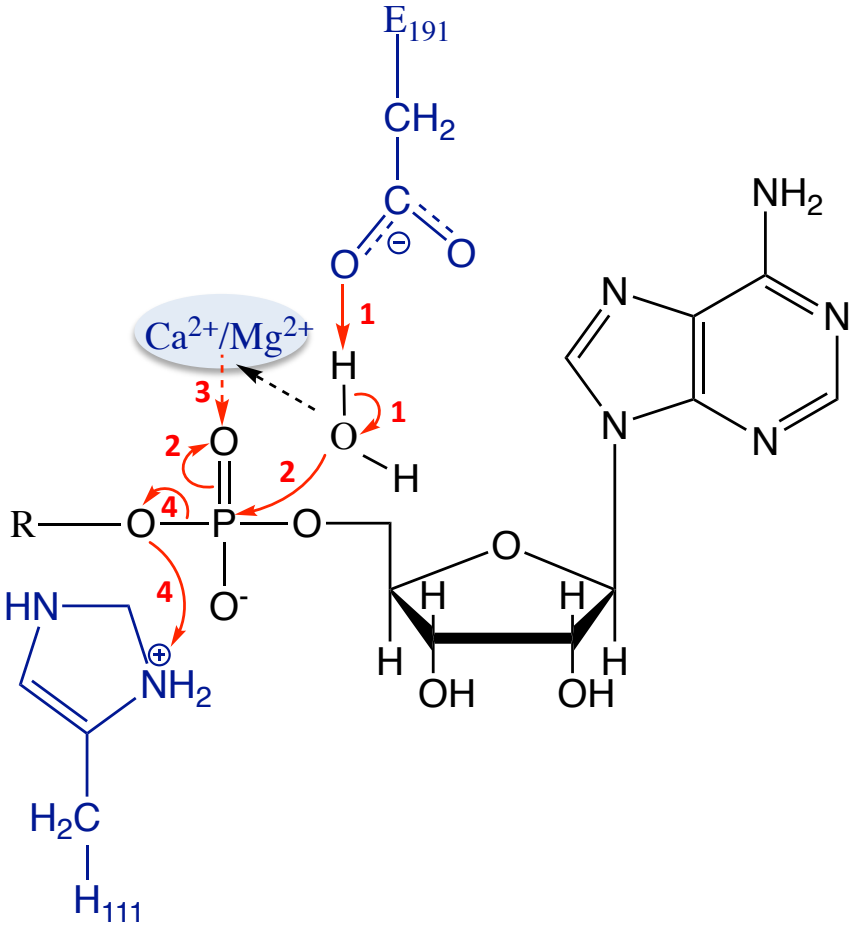

E191
CH2
C
O
O
1
Ca2+/Mg2+
H
3
1
2
O
O
H
2
R
O
4
P
O
O-
4
HN
NH2
H2C
H111
O
H
H
H
H
OH
OH
NH2
N
N
N
N

Figure 5